ACS APPLIED MATERIALS & INTERFACES

Research Article

www.acsami.org

Carbon Nitrogen Nanotubes as Efficient Bifunctional Electrocatalysts for Oxygen Reduction and Evolution Reactions

Ram Manohar Yadav,[†,‡] Jingjie Wu,[†] Raji Kochandra,[†] Lulu Ma,[†] Chandra Sekhar Tiwary,[†] Liehui Ge,[†] Gonglan Ye,[†] Robert Vajtai,[†] Jun Lou,*[,†] and Pulickel M. Ajayan*[,†]

[†]Department of Materials Science and NanoEngineering, Rice University, Houston, Texas 77005, United States

[‡]Department of Physics, VSSD College, Kanpur, 208002, India

Supporting Information

ABSTRACT: Oxygen reduction and evolution reactions are essential for broad range of renewable energy technologies such as fuel cells, metal-air batteries and hydrogen production through water splitting, therefore, tremendous effort has been taken to develop excellent catalysts for these reactions. However, the development of cost-effective and efficient bifunctional catalysts for both reactions still remained a grand challenge. Herein, we report the electrocatalytic investigations of bamboo-shaped carbon nitrogen nanotubes (CNNTs) having different diameter distribution synthesized by liquid chemical vapor deposition technique using different nitrogen containing precursors. These CNNTs are found to be efficient bifunctional electrocatalyst for oxygen reduction and evolution reactions. The electrocatalytic activity strongly depends on the nanotube diameter as well as nitrogen functionality type. The higher diameter CNNTs are more favorable for these reactions. The increase in nanotube diameter itself enhances the catalytic activity by lowering the oxygen adsorption energy, better conductivity, and further facilitates the reaction by increasing the percentage of catalytically active nitrogen moieties in CNNTs.

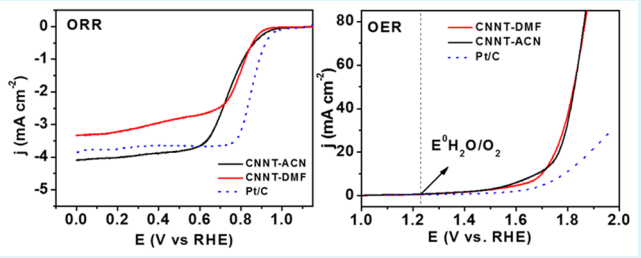

KEYWORDS: *carbon nitrogen nanotubes, nitrogen moieties, nanotube diameter, oxygen reduction and evolution reactions*

1. INTRODUCTION

The conventional remnant fuels brings the prosperity in our society by providing us chemical energy; although, the illimitable energy consumption instigates the fast diminution of conventional fossil fuels and enhances environmental pollution. The highly efficient renewable energy systems (e.g., fuel cells, metal−air batteries) are extremely desirable to fulfill the need and utilization of sustainable energies.[1,2] Electrode catalysts for oxygen reduction reaction (ORR) and oxygen evolution reaction (OER) play a key role in wide range of renewable energy technologies. Elaborating highly active electrocatalysts for ORR and OER has got immense attention from researchers because of the lethargic kinetics of these two reactions, which causes critical energy efficiency loss, restricts the accomplishment/performance and commercialization of fuel cells and metal-air batteries.[3] Metal-based materials (such as Pt and its alloys for ORR, ruthenium (Ru), iridium (Ir), and cobalt (Co) oxides for OER) were extensively studied as oxygen electrode catalysts because of their high activity[4−6] but their use is still limited becaue of scarce availability, poor stability, and high cost.[7] Therefore, extensive research efforts have been taken to develop alternative low-cost and high-performance oxygen electrode catalysts with improved efficiency and stability.[8] In addition, the Pt electrode is good for ORR but not for OER and ruthenium/iridium oxides are good for OER but not for ORR. Therefore, bifunctional electrocatalysts are highly desirable for regenerative fuel cell and metal−air battery for the replacement of conventional costly metals.

In this regards, the heteroatom (especially nitrogen) doped carbon nanostructures have emerged as a new electrocatalyst system for ORR due to their low cost, high activity and excellent durability.[9−22] Recently, nitrogen-doped carbon nanomaterials were investigated as an efficient oxygen evolution electrocatalysts.[2,23,24] These studies revealed that the nitrogen doped carbon nanostructures can perform as a bioperational catalysts for ORR and OER. Researchers studied the factors governing the catalytic activity of nitrogen-doped carbon nanotubes (e.g., total nitrogen content and their bonding configurations with other parameters in the nanotubes) but the origin of catalytic activity is not fully explained. It is evident that the insertion of nitrogen in the carbon nanotubes (CNTs) induces active sites that can participate in breaking the O−O bonds of oxygen molecules.[9] Sharifi et al.[25] studied the role of different type of nitrogen functionality (e.g., pyridinic, pyrrolic, quaternary center, and quaternary valley) on the catalytic

Received: March 7, 2015
Accepted: May 13, 2015
Published: May 13, 2015

DOI: 10.1021/acsami.5b02032
ACS Appl. Mater. Interfaces 2015, 7, 11991−12000

activity of nitrogen doped CNTs toward ORR and concluded that the catalytic activity is connected with all types of nitrogen functionality but the most active one is quaternary valley (N-Q_{valley}), followed by pyridinic. They also related the number of electrons involved in the reaction process with type of nitrogen functionality and reported that the ORR process takes place by a direct four-electron pathway for the N-Q_{Valley} and the pyridinic sites while it proceeds by an indirect two-electron pathway on quaternary center (N-Q_{center}) sites. Niwa et al.[26] reported the higher ORR activity with a larger amount of graphite/quaternary nitrogen than those with a larger amount of pyridine nitrogen. On the other hand, some researchers[27,28] have shown that pyridinic nitrogen moieties are more efficient than N-Q_{valley} in nitrogen doped CNTs. The role of particular nitrogen functionality is still under debate with consensus that the most active one is in between pyridinic and N-Q_{Valley} nitrogen. It appears that in addition to only nitrogen moieties, some other factors also affect the electrocatalytic activity of nitrogen doped CNTs. In this regard, Kaukonen et al.[29] studied the effect of nanotubes diameter on the catalytic activity of nitrogen doped CNTs. On the basis of their theoretical calculations, they reported that in spite of only type of nitrogen functionality the nanotube diameter is also play a role in ORR. But the experimental verification of their calculation is still lacking. Keeping this in view, we have synthesized the carbon nitrogen nanotubes (CNNTs) with different diameters by varying the precursors and growth conditions. Moreover, the effect of nanotube diameter with nitrogen functionality on the electrocatalytic activity of CNNTs toward ORR and OER is systematically analyzed. This study illuminates the principle of choosing right precursors and synthesis conditions to synthesize CNNTs for desired catalysts applications.

2. EXPERIMENTAL SECTION

2.1. Synthesis of CNNTs. The CNNTs have been synthesized on large scale by the liquid CVD using nitrogen containing hydrocarbons with ferrocene in Ar/H_2 atmosphere at elevated temperatures. For the present work we have chosen acetonitrile (ACN), dimethylformamide (DMF), triethylamine (TEA), and hexamethylenetetramine (HMTA) as precursors. The concentration of ferrocene in precursors kept at 5 mg/mL found best per our previous publication.[30] The temperature for the synthesis of C−N nanotubes varied from 650 to 1000 °C but we got good quality nanotubes without other carbonaceous materials in between 750 and 950 °C. The quartz tube with diameter 5 cm and length 1 m was placed in a three zone horizontal furnace with the heating zone of 81 cm. The furnace was heated at the rate of 40 °C/min to desired temperature from the room temperature under the argon ambience. When the optimum temperature reached, the precursors were injected by the vacuum-tight syringe in the quartz tube with the flow rate of 12 mL/h in Ar/H_2 atmosphere. We have varied the flow rate from 6 to 18 mL/h and found 12 mL/h as the suitable one for yield. The flow rate of Ar/H_2 was kept at 1000 sccm with argon to hydrogen ratio of 80:20 for all the experiments. The deposited materials ware collected from the quartz tube and heat treated in air for 3 h at 360 °C to become free from other carbonaceous materials.

2.2. Structural and Microstructural Characterizations. The microstructure of the materials were characterized by scanning electron microscope (FEI Quanta 400 FEG ESEM) and high resolution field emission gun transmission electron microscope (JEOL 2100 FEG TEM). The Raman spectra were taken from Renishaw inVia Raman microscope with 514 nm laser excitation. X-ray photoelectron spectrometer on PHI-5000C ESCA system with Al Ka X-ray as an excitation source was used to analyzed the chemical nature and composition of the materials.

2.3. Electrochemical Measurements. We have prepared different electrodes for electrocatalytic measurements under the similar experimental conditions. Working electrodes were prepared by the following way. 1.6 mg of CNNTs samples were dispersed in a solution containing 125 μL of deionized water, 75 μL of isopropanol and 20 μL of 0.5 wt.% Nafion dispersion. To prepare a homogenized catalysts ink the mixtures were ultrasonicated for 30 min then 8 μL of 7.27 mg mL^{-1} CNNTs ink was dropped onto the disk glassy carbon electrode of rotating ring disk electrode (RRDE) and dried in the vacuum oven at 60 °C. Pt/C (20 wt. %) electrode was prepared under the similar method. The Pt loading on the GC electrode was 36 μg cm^{-2}.

The electrochemical measurement was carried out in an Autolab PDSTAT302N electrochemical station equipped with a typical three-electrode configuration accompanied by gas flow systems. Ag/AgCl (Saturated KCl) was used as reference electrode and Pt wire as counter electrode. 0.1 M KOH aqueous solution has been taken as electrolyte for both normal cyclic voltammogram (CV) and RRDE voltammogram measurements. Prior to every experiment, an Ar or O_2 flow was used through the electrolyte for at least 30 min. The CV was performed from −1.2 to 0.2 V vs Ag/AgCl with a sweep rate of 50 mV s^{-1}. For ORR, RRDE polarization curves were measured by sweeping the disk electrode potential cathodically from 0.2 V to −1.0 V vs Ag/AgCl at 5 mV s^{-1} while the platinum ring electrode potential was kept constant at 0.3 V vs Ag/AgCl for oxidizing the HO_2^- intermediate. The collected background currents in O_2 saturated electrolyte were removed to eliminate capacitive contributions. The onset potentials were determined from the intersection of the two tangents drawn at the rising current and the background current of the polarization curves. For OER, the RRDE measurement was performed at 1600 rpm, and the polarization curves were IR drop corrected by measuring the ohmic resistance from the electrochemical impedance spectroscopy. In the main text the potential was rescaled to reversible hydrogen electrode, $E_{RHE} = E_{Ag/AgCl} + 0.20 + 0.0591$ pH.

The comprehensive numbers of electron per oxygen molecule transferred in ORR were calculated from the slopes of Koutecký−Levich (K−L) plots using the equation

$$\frac{1}{j} = \frac{1}{j_k} + \frac{1}{j_d} = \frac{1}{nFkC_{O_2}^b} + \frac{1}{0.2nFD_{O_2}^{2/3}\nu^{-1/6}C_{O_2}^b\omega^{1/2}} \quad (1)$$

where j is the measured current, j_k and j_d are the kinetic and diffusion-limiting current densities, respectively, k is the rate constant for ORR, F is the Faraday constant (96 485 C mol^{-1}), ω is the rotation speed (rpm), D_{O_2} is the diffusion coefficient of oxygen (1.9×10^{-5} cm^2 s^{-1}),[31] $C_{O_2}^b$ is the bulk concentration of oxygen (1.21×10^{-6} mol cm^{-3}),[31] and ν is the kinematic viscosity of the solution (0.01 cm^2 s^{-1}).[32] The second way to calculate n is to use the ring current and the disk current at a specific potential.[25]

$$n = \frac{4I_D}{I_D + \frac{I_R}{N}} \quad (2)$$

$$\%HO_2^- = \frac{100(4-n)}{2} \quad (3)$$

I_D and I_R are the disk and ring currents, respectively, and $N = 0.25$ is the collection efficiency for hydrogen peroxide in the RRDE.

3. RESULTS AND DISCUSSION

CNNTs were synthesized by liquid CVD method using ACN, TEA, NMF, and HMTA as C/N precursors and ferrocene as catalyst precursor. A massive black deposition takes place along the total heating zone inside the quartz tube by injecting the precursor's solution in Ar/H_2 ambience at elevated temperatures (750, 850, and 950 °C). After the growth, CNNTs were collected from the walls of the quartz tube and further annealed in air at 360 °C for 3 h to remove the other carbonaceous species. Microscopic exploration revealed the formation of

DOI: 10.1021/acsami.5b02032
ACS Appl. Mater. Interfaces 2015, 7, 11991−12000

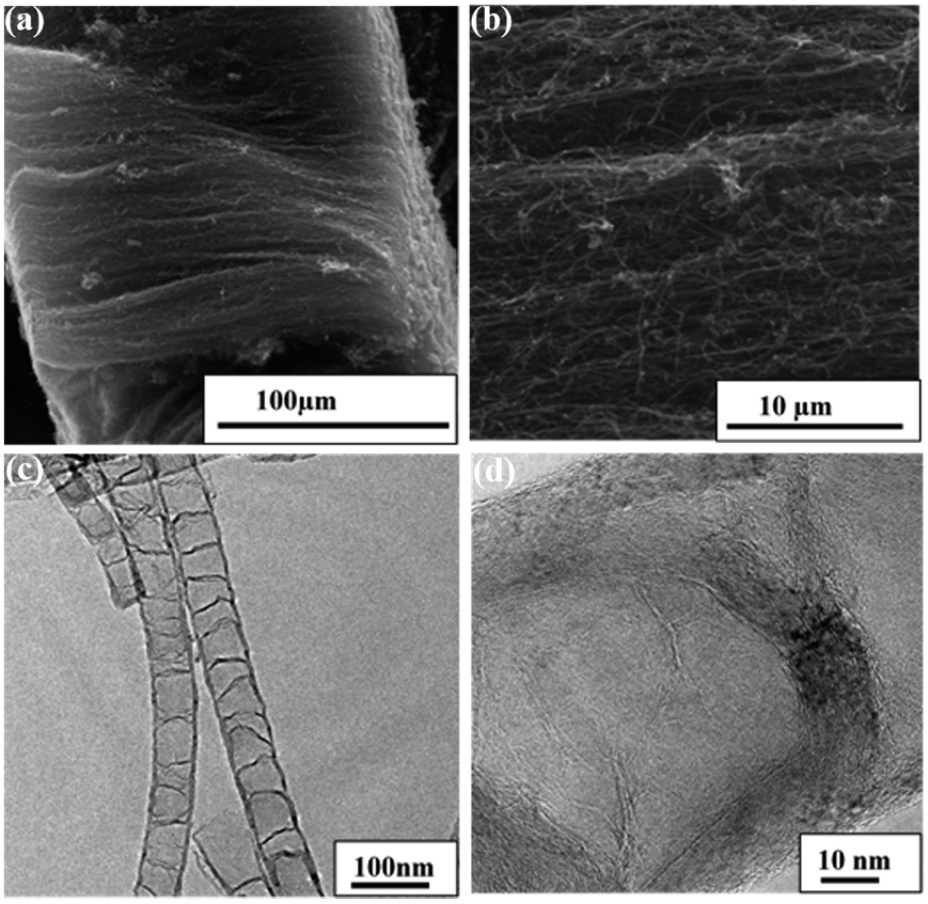

Figure 1. Electron microscopic characterizations of CNNTs. Representative SEM images (a, b), low-magnification (c), and high resolution TEM (d) of CNNTs synthesized with ACN precusor.

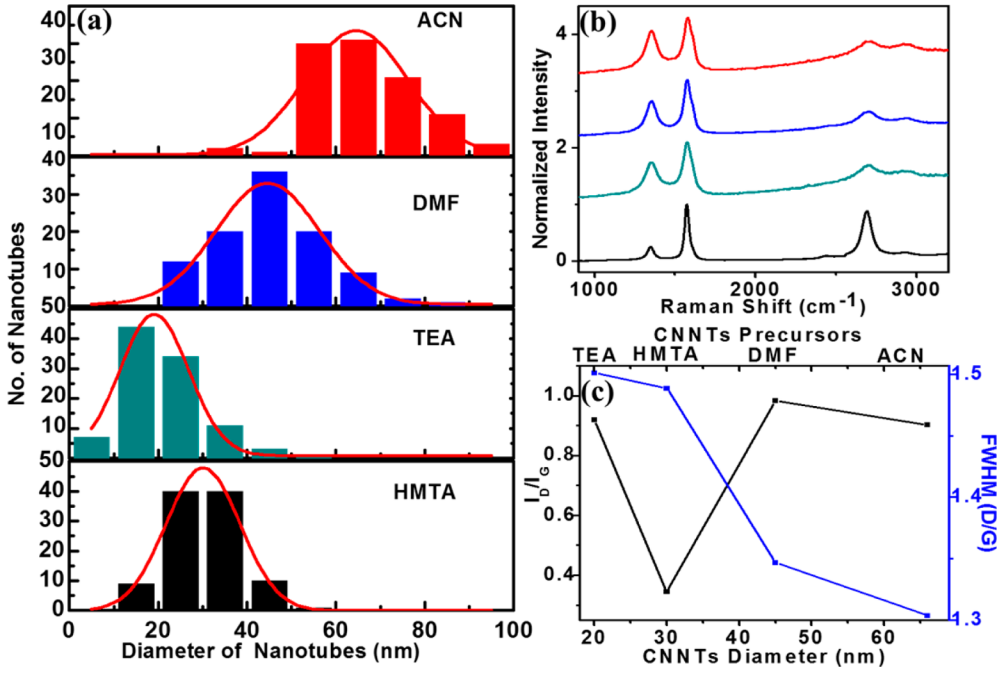

Figure 2. Structural characterization of CNNTs. Diameter dristribution variation with precorsors (a). Raman spectra of as synthesized CNNTs at 850 °C (b). Variation of I_d/I_g and $fwhm_D/fwhm_G$ with diameter and precursors (c).

clean, well aligned CNNTs with all the precursors having almost similar morhology. Figure 1a and b shows the representative SEM images of as synthesized CNNTs. Figure 1c and d shows the typical TEM images, showing the CNNTs

DOI: 10.1021/acsami.5b02032
ACS Appl. Mater. Interfaces 2015, 7, 11991−12000

are multiwalled with bamboo-shaped morphology and free from other carbonaceous materials. An interesting observation from the microscopic investigations shows that the diameter of the CNNTs varied with changing the precursor solution as shown in Supporting Information Figure S1a–d. The mean diameter of the CNNTs are 20, 31, 45, and 66 nm with TEA, HMTA, DMF, and ACN, respectively. The variation in diameter dristribution is plotted in Figure 2a. The mean diameter of the CNNTs also slighlty increases with increase in growth temperature with a specific precursor as reported in our earlier publication.[33]

Raman spectroscopy has been extensively used to analyze the crystallinity and the disorder in carbon nanostructures.[34−38] Raman spectra of the CNNTs grown with different precursors are shown in Figure 2b. The strong band around 1584 cm^{-1}, which is known as the G-band, arises from a Raman-allowed G-point vibration related to the optical phonon modes of E_{2g} symmetry in graphite and known as tangential mode for carbon nanotubes.[34,35] The D-band at around 1355 cm^{-1}, which comes from defects in the curved graphene sheets, tube ends, or from the doping of heteroatoms in carbon network,[36] is correspondent with optical phonons close to the K-point of the Brillouin zone in graphite and carbon nanotubes. The integrated intensity of D mode is generaly normalized with respect to that of the G mode for estimating the defect concentration.[39,40] For CNNTs, variations in chemical bond lengths and atomic masses of carbon and nitrogen as well as the pentagons formation lead to local distortion in the graphite sheets. Therefore, the intensity ratio of the D to G modes (I_d/I_g) is considered to be related to the defect fraction originating from nitrogen incorporation and might be considered as a approximate measure of the degree of nitrogen hybridization.[30,41]

The value of I_d/I_g for the as grown CNNTs is plotted in Figure 2c. It is clear that the I_d/I_g value does not rely on CNNTs diameter variation but sensitive to structural defects and varies with the variation in nitrogen concentration (Figure 3f).The Raman peak bandwidth is highly sensitive to strain effects in sp^2 nanocarbons and can be used to probe strain modification in the microstructure. Curvature effects due to nanotube diameter gives the multiple peaks or broadening of bandwidth.[37] Antunes et al.[42] reported that the ratio of D and G bandwidth is sensitive to the nanotube diameter distribution and decreases with the increase in tube diameter. In our case the Raman spectroscopic analysis reveals very interesting correlations between $fwhm_D/fwhm_G$ (D band full width at half-maximum normalized with respect to G band full width at half-maximum) and CNNTs diameter. The $fwhm_D/fwhm_G$ of the CNNTs decreases with increasing nanotube diameter as shown in Figure 2c. The $fwhm_D/fwhm_G$ is also the measure of defects in CNNTs, but it seems that the normalized fwhm of D band depends greatly on modifications in microstructures due to strain produced by curvature of the nanotubes rather than structural defects induced by nitrogen incorporation. As the diameter of the nanotubes increases, the strain instigate by the curvature effect[37] dwindles and thus this ratio decreases. Supporting Information Figure S2a shows the Raman spectra with the ACN precursor at different growth temperature. The $fwhm_D/fwhm_G$ also decreases with growth temperature because the diameter of the nanotubes increases slightly with increase in growth temperature (Supporting Information Figure S2b).[33]

The stoichiometric composition and chemical bonding states of the as-grown nanotubes were analyzed by X-ray photoelectron spectroscopic (XPS) technique. The survey scans of CNNTs synthesized using different precursors as shown in Supporting Information Figure S3, confirm the presence of both carbon and nitrogen in CNNTs while did not show any peak for Fe indicating a ultralow content of Fe residue. The high resolution XPS spectra (Figure 3) shows the preseance of different N species. Figure 3a shows the C 1s peak at 284.5 eV and Figure 3b–e shows N 1s peaks arround 398.5, 400.8, and 401.5 eV with three types of nitrogen configarations of piridinic, pyrrolic and graphitic nitrogen respectively for all precursors. The total nitrogen percents in the CNNTs synthesized at 850 °C are 2.4, 2.9, 2.4, and 0.3 at. % with ACN, DMF, TEA, and HMTA, respectively, as shown in Figure 3. The nitrogen content decreases slighlty with increase in temperature. An interesting correlation between diameter of the nanotubes and type of nitrogen content has been stablished by TEM and XPS investigations. It was found that with the increase in CNNTs diameter the percentage of pyridinic nitrogen (398.5 eV) present in the nanotubes keep increasing and graphitic nitrogen (401.1 eV) is almost constant with slight increment, whereas the pyrrolic nitrogen (400.4 eV) decreases rapidly as shown in Supporting Information Table S1.The reason for this variation is not yet clear but it seems that the presence of excess pyrrolic nitrogen (means more pentagon in graphetic network) facilitates the formation of lower diameter nanotubes. This is because of the fact that the formation of curvature is easy with the presence of pentagon in spite of only hexagon in graphetic network. We also have found similar decrease in pyrrolic nitrogen and consequently increase in

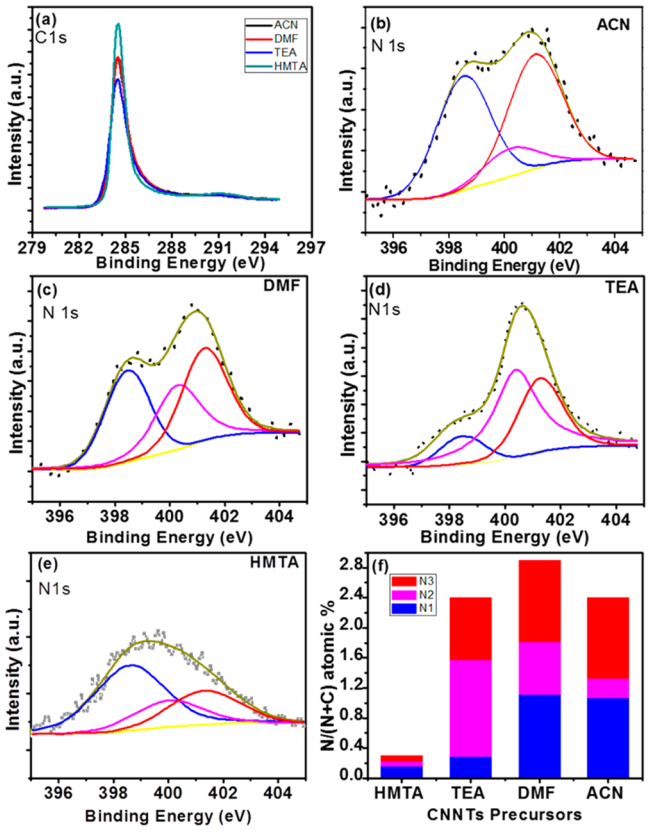

Figure 3. XPS spectra of C 1s (a) and N 1s (b–e) of CNNTs synthesized employing various precursors. Variation of N contents with CNNTs precursors (f). N1, N2, and N3 stand for pyridinic, pyrrolic, and graphitic nitrogen, respectively.

DOI: 10.1021/acsami.5b02032
ACS Appl. Mater. Interfaces 2015, 7, 11991−12000

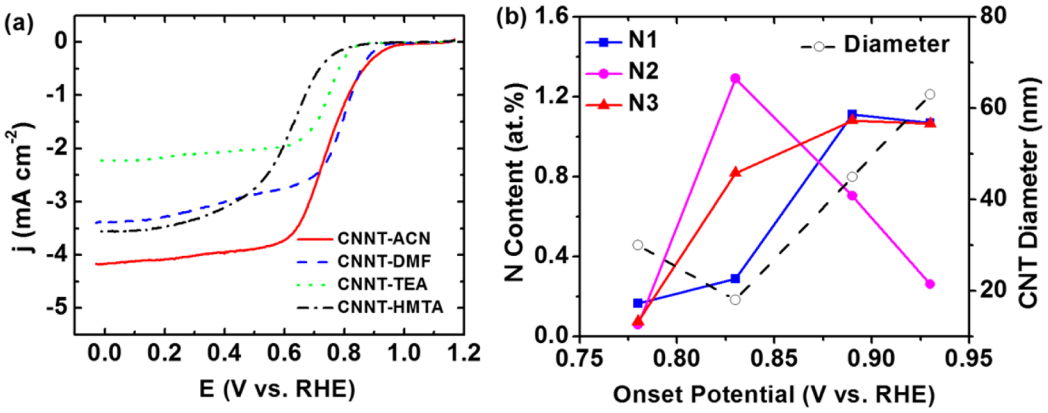

Figure 4. Comparison of electrochemical activity of CNNTs synthesized by different precursors. Steady-state polarization curves (a) and the dependence of onset potential on N distribution and tube diameter (b). N1, N2, and N3 stand for pyridinic, pyrrolic, and graphitic nitrogen, respectively.

pyridinic nitrogen with graphetic nitrogen almost constant when growth temperature increases from 750 to 850 °C. Although when we further increase the temperature to 950 °C the graphatic nitrogen content increases with decrease in both pyrrolic and pyridinic nitrogen (Supporting Information Figure S4).

The electrocatalytic activity of CNNTs toward ORR was examined in a conventional three-electrode electrochemical cell with a RRDE as the working electrode in O_2 saturated 0.1 M KOH solution. We did the electrochemical characterization of CNNTs prepared at different temperature and found that CNNTs prepared at 850 °C are the most active (Supporting Information Figure S5). Thus, we have chosen these CNNTs produced at 850 °C for further study. Regarding to the effect of precursor, the CNNT-ACN exhibits the highest performance indicated by the most positive onset potential of 0.93 V vs RHE, followed by CNNT-DMF (0.89 V), CNNT-TEA (0.83 V), and CNNT-HMTA (0.78 V) (Figure 4a). In addition, CNNT-ACN has the largest diffusion-limiting current density.

We have compared the performance of CNNT-ACN activity toward ORR to recently reported data in reputed journals and found that it is better than various reported results on NCNTs,[21,43,44] NCNTs/graphene composites[2] and comparable to data reported by Gong et al.[9] on vertically aligned NCNTs and Cheng et al.[45] on winged NCNTs. Gong et al. studied ORR on vertically aligned N doped CNTs directly grown on electrode while Cheng et al. unzipped the outer wall of N-doped CNTs to increase the surface area of electrocatalysts for ORR. Both these methods are complicated than ours. Since the discovery of N-doped carbon nanotubes as electrocatalysts toward ORR, the role of N moieties as the catalytic active site has been under debate in both theoretical and experimental research.[25−28] The most controversial issue lies in whether the activity comes from the pyridinic-N or graphitic-N. To achieve efficient ORR, it requires that the active sites exhibit a relatively low binding energy for the oxygen but yet a high electron density localized around the active catalytic site to mediate the electron transfer.[29,46] The graphitic-N in the valley sites is calculated to lower the O_2 adsorption barrier to carbon neighboring the valley N and enhances O_2 reduction to H_2O via a 4-electron reduction pathway.[47,48] Some experimental results support the modeling conclusion.[25,49] In many studies, the graphitic-N in the basal planes and in the valley sites are not distinguishable and are classified into graphite-N which plays an important role for the ORR activity.[50−53] The relative electronegativity of graphitic-N atoms reduces the electron density on the adjacent C nuclei, which helps electrons transfer from the adjacent C to N atoms, and N back-donates electrons to adjacent carbon p_z orbitals. The donation and back-donation processes not only facilitate O_2 dissociation on the adjacent C atoms, but also help forming a strong chemical bond between O and C.[51−53] While the density functional theory (DFT) modeling also shows that pyridinic-N induces either high positive spin density or high positive atomic charge density to adjacent carbon atom to weaken the O−O bond via the bonding between oxygen and carbon atom, and thus facilitate the 4-electron reduction process.[54] A lot of experimental results prove pyridinic-N is ORR active.[27,28,43,55,56] In our case, the pyrrolic-N is excluded as the most active site due to the observation that the activity increases with the decrease of pyrrolic-N atomic content (Figure 4b). Our results shows that the primary activity comes from both graphitic-N and pyridinic-N but we cannot distinguish between them, because the trend is similar showing the ORR activity increases with the increase of graphitic-N and pyridinic-N atomic content except for CNNT-ACN (Figure 4b). Although the graphitic-N or pyridinic-N atomic content in CNNT-ACN is slightly lower than that in CNNT-DMF, the onset potential is a little more positive. This is attributed to the effect of CNNT diameter. The limiting current density increases with increase in diameter of the nanotubes (as shown in Figure 4a). Larger tube diameter has lower O_2 adsorption energy which contributes to the positive shift of onset potential.[29] Kaukonen et al.[29] did the computational study on the role of tube diameter for ORR on CNNTs and interpreted that the high catalytic activity occurs only when the radius of the NCNTs is large enough based on the calculated combination of the low formation energy of the defect and the weak binding of oxygen to it. The conductivity of carbon nanotubes depend on their diameter and it is well-known that higher diameter nanotubes having more number of metallic nanotubes than lower diameter nanotubes[57−59] and thus enhancing overall conductivity of the CNNTs catalysts. This increased conductivity may also contributes to higher electrochemical performance of CNNTs.

The complete removal of Fe particles is not possible from CVD synthesized CNNTs. However, equal and least catalysts concentration was taken during CNNTs growth for all

DOI: 10.1021/acsami.5b02032
ACS Appl. Mater. Interfaces 2015, 7, 11991−12000

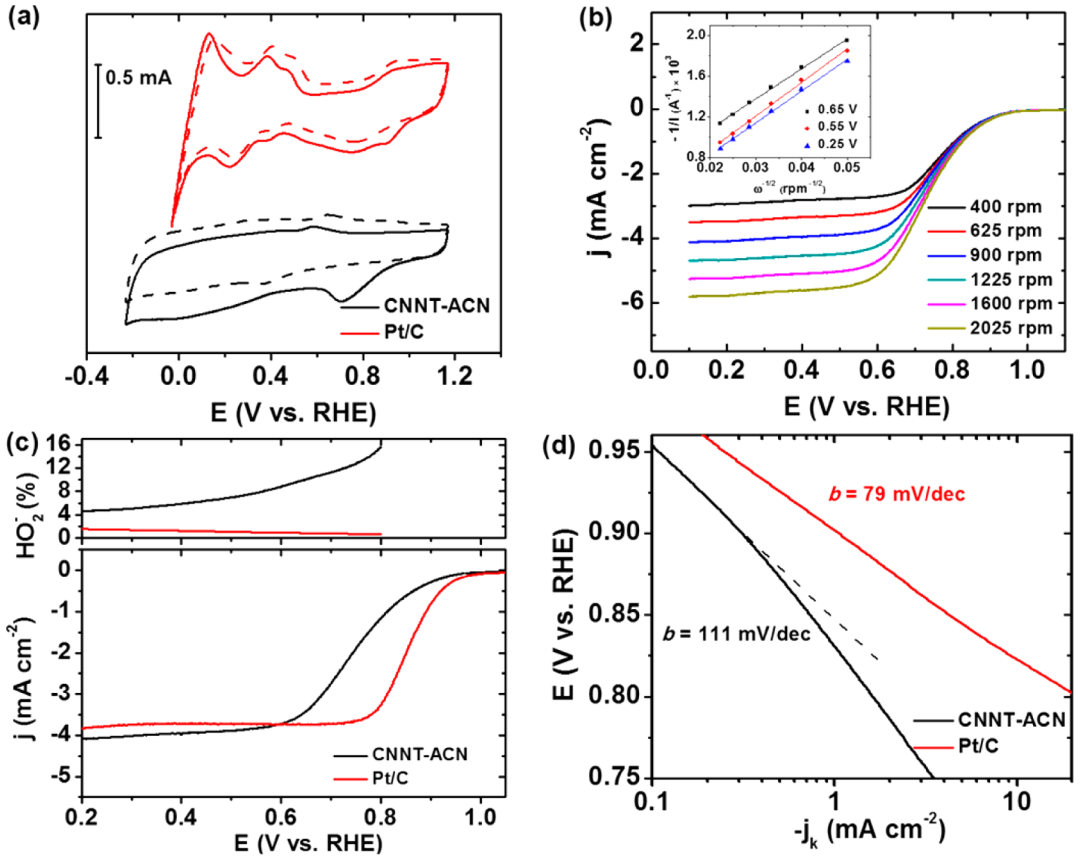

Figure 5. Electrocatalytic activity toward ORR of CNNT-ACN. Cyclic voltammetry of CNNT-ACN and Pt/C in Ar (dash line) and O_2 (solid line) saturated 0.1 M KOH (a). Polarization curves at different rotating speeds for CNNT-ACN (b). Inset is the Koutecký–Levich plots. RRDE polarization curves and peroxide yield of CNNT-ACN and Pt/C at a rotating speed of 900 rpm (c). Tafel curves of CNNT-ACN and Pt/C after mass-transport correction (d).

precursors so the iron content is low and almost same in all samples. In addition, all samples are acid treated before electrochemical measurements to remove the Fe particles. The CVs of our CNNT samples (Supporting Information Figure S6) show no prominent peak for Fe redox reactions. The role of trace metal (Fe in our case) in the catalytic activity of ORR is still under debate. To elaborate our understanding on this issue we also run ORR on the single walled carbon nanotubes (CNTs, HiPco) having high concentration of Fe species. The CVs of CNTs show a couple of peaks at 0.49 and 0.14 V attributed to redox reactions associated with the Fe catalyst residues. The CNTs contains much more Fe residues as indicated by the peak current density as compared to that of CNNTs (Supporting Information Figures S7a and S6). However, the CNTs exhibit much lower activity toward ORR than CNNTs samples. For example, the ORR peak potential in the CVs for CNTs is 0.57 versus 0.78 V for the least active CNNT-HMTA (Supporting Information Figures S7a and S6). In addition, the onset potential for CNTs is less positive than all CNNTs, for example. 0.69 V for CNTs versus 0.78 V for the least active CNNTs-HMTA (Supporting Information Figure S7b). From RRDE results, the CNTs yield more HO_2^- than CNNTs, for example, 40% for CNTs versus 10% for CNNT-ACN at 0.6 V (Supporting Information Figure S7c and Figure 5c). These results indicate negligible contribution of Fe residues to the ORR activity. Thus, a trace amount of Fe species in our CNNTs would not affect our discussion on the effect of N configuration and nanotube diameter on the catalytic activity.

The performance CNNT-ACN electrode was further evaluated as compared to commercial 20 wt % Pt/C (Johnson Matthey). The CNNT-ACN electrode exhibits a pronounced cathodic ORR peak at 0.70 V when the electrolyte of 0.1 M KOH is saturated with O_2 (Figure 5a). The high ORR activity is also shown in its onset potential (~0.93 V) and half-wave potential ($E_{1/2} \approx 0.74$ V) in the RRDE polarization curves (Figures 4a and 5b and c). Koutecký–Levich (K–L) plots j^{-1} versus $\omega^{-1/2}$ derived from the polarization curves at the rotating speed ranging from 400 to 2025 rpm is linear, suggesting first-order reaction kinetics toward the concentration of dissolved oxygen (Figure 5b and inset).[60] According to the K–L equation, the average electron number (n_e) per oxygen molecule transferred during ORR was calculated to be around 4.0 at the potential ranging from 0.65 to 0.25 V.[60,61] The HO_2^- yield decreases from ~15% at 0.80 V to ~5% at 0.25 V (Figure 5c). Normally the ring disk current increases along with the decrease of potential. However, the decrease of peroxide yield happens on carbon materials as the potential decreases because more O_2 is directly reduced to OH^- or H_2O.[62,63] The n_e from the HO_2^- yield ($n_e = 4(\% HO_2^-)/50$) is 3.7–3.9 when potential sweeps from 0.80 to 0.25 V, indicating oxygen reduction proceeds via a 4-electron pathway on CNNT-ACN. Kinetic currents derived from the mass transport correction of the disk currents (Figure 5d) show a Tafel slope of ~110 mV/dec in the low overpotential region, which directly corresponds

DOI: 10.1021/acsami.5b02032
ACS Appl. Mater. Interfaces 2015, 7, 11991–12000

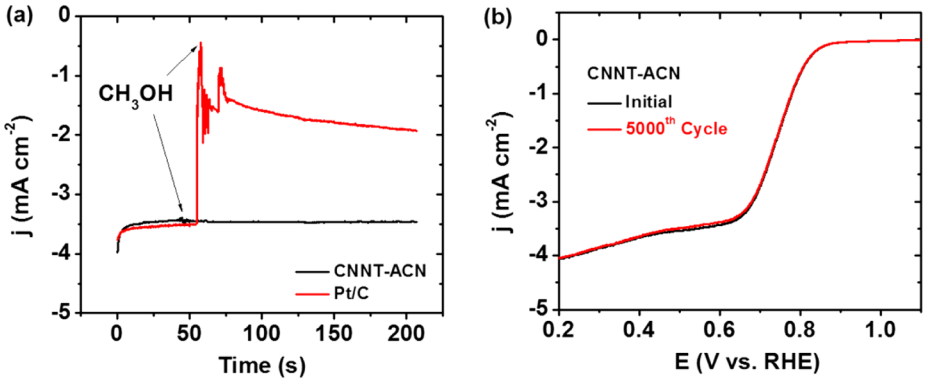

Figure 6. Long time stability and tolerance to alcohol poisoning. The ORR cathodic current−time response at CNNT-ACN and Pt/C (20%) electrodes at 0.5 V in O_2 saturated 0.1 M KOH before and after adding 0.5 M methanol (a). The polarization curves of CNNT-ACN before and after 5000 cycles (b).

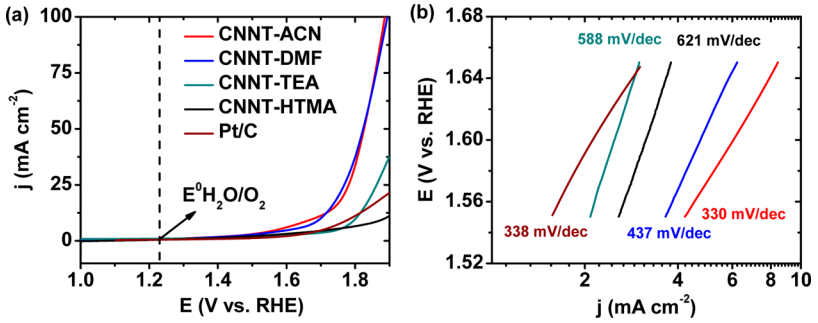

Figure 7. Performance of CNNTs for OER. Polarization curves of OER for commercial Pt/C (20 wt.%) and CNNTs electrodes in 0.1 M KOH solution at a scan rate of 5 mV s^{-1} and rotating speed 1600 rpm (a). Tafel plots of Pt/C (20 wt. %) and CNNTs (b).

to a chemical rate-determining step, for example, O_2 adsorption onto the surface of the CNNTs, compared to a first electron transfer rate-determining step for the Pt/C catalyst as indicated by the Tafel slope of 79 mV/dec.[64−66]

The resistance to crossover of methanol was evaluated in the chronoamperometry by adding 0.5 M methanol into the electrolyte of 0.1 M KOH. The corresponding *j*−*t* response for CNNT-ACN maintains stable, suggesting its tolerance to alcohol fuel, while the Pt/C electrode is subjected to a sharp decrease in current up to 70% upon the addition of 0.5 M methanol as shown in Figure 6a. The polarization curve for CNNT-ACN also remains intact after introducing the methanol (Supporting Information Figure S8). The durability of CNNT-ACN was assessed according to the accelerated durability test protocol by continuous cycling the catalysts in the potential window of 0.6−1.0 V at 50 mV s^{-1} under O_2 atmosphere for 5000 cycles. The CNNT-ACN exhibits excellent durability during the cycling as shown in the overlap of polarization curves for CNNT-ACN before and after 5000 cycles as shown in Figure 6b. The CNNT-ACN shows more stable performance than Pt/C which experiences a decrease of $E_{1/2}$ by 20 mV after analogous accelerated potential cycling test (Supporting Information Figure S9).

We have also evaluated the electrocatalysis of OER on CNNTs by extending the potential to the water oxidation regime. In 0.1 M KOH, the CNNT-ACN and CNNT-DMF exhibit the similar electrocatalytic activity toward OER and afford much higher OER currents than the CNNT-TEA, CNNT-HTMA, and Pt/C. The potential at 10 mA cm^{-2}, a criterion commonly used to judge the OER activity, is smaller for CNNT-ACN (1.68 V) and CNNT-DMF (1.70 V) compared to CNNT-TEA (1.80 V) and CNNT-HTMA (1.89 V) and Pt/C (1.78 V) as shown in Figure 7a. The OER activity of CNNT-ACN is comparable to that of nitrogen-doped graphene/carbon nanotube hybrid materials and approaching to the IrO_2/C catalysts.[2,23] The CNNT-ACN catalyst generated a current density of 10 $mAcm^2$ at a potential of 1.68 V (Figure 7a), which is nearby to that of reported highest active IrO_2/C, 1.60 V, by Zhao et el.[23]

The Tafel slope of CNNT-ACN is the smallest among these CNNT samples with similar trend to overpotential as shown in Figure 7b. However, the Tafel slope value (330 mV/dec) for CNNT-ACN is still large, which needs further improvement. There are various reports on OER application of N doped carbon nanostructures in which only some of them discuss about Tafel plot.[2,14,67−69] Actually there is a huge range in Tafel slope from 658[67] to 83 mV/dec[2] in reported papers. The large difference of Tafel slopes suggests a variety of reaction mechanisms because of the complexity of N doped carbon nanostructures in N functionality distribution, nanotube size and number of walls, chirality, graphene layers, and surface functional groups. OER measurements revealed that the overpotential needed for OER and Tafel slop both decreases with increase in nanotube diameter (Figure 7), which confirms the suitability of higher diameter nanotubes for OER activity, similar to ORR. We got best performance bifunctional electrocatalysts with larger diameter CNNTs synthesized by ACN and worse in case of smaller diameter CNNTs synthesized by HMTA and TEA despite having similar N content in case of CNNTs obtain from TEA. By choosing suitable precursor, the CNNTs are a powerful bifunctional catalyst for both oxygen reduction and water oxidation.

DOI: 10.1021/acsami.5b02032
ACS Appl. Mater. Interfaces 2015, 7, 11991−12000

4. CONCLUSIONS

We have synthesized CNNT samples with varying diameter having similar nitrogen content by liquid CVD method using different precursors. These CNNTs are low cost and efficient bifunctional catalyst both for ORR and OER with high activity, excellent durability and resilience to methanol crossover. The CNNT-ACN exhibits the highest performance for both ORR and OER followed by CNNT-DMF, CNNT-TEA, and CNNT-HMTA. Our results elucidate the dependence of electrocatalytic activity not only on N moiety types but also on diameter of these nanotubes. The larger diameter of the nanotubes synergizes the catalytic activity of these CNNTs originating from the nitrogen moieties by lowering oxygen adsorption energy and enhanced conductivity. The design of efficient bifunctional catalysts can be achieved by choosing the precursor to tune both of these two factors.

■ ASSOCIATED CONTENT

Supporting Information

Physical characterization of CNNTs, more electrochemical tests of CNNTs, CNTs, Pt/C electrodes. The Supporting Information is available free of charge on the ACS Publications website at DOI: 10.1021/acsami.5b02032.

■ AUTHOR INFORMATION

Corresponding Authors

*E-mail: jlou@rice.edu.
*E-mail: ajayan@rice.edu.

Author Contributions

R.M.Y. and J.W. contributed equally to this work.

Notes

The authors declare no competing financial interest.

■ ACKNOWLEDGMENTS

The authors acknowledge the financial support from U.S. Air Force Office of Scientific Research for the Project MURI "Synthesis and Characterization of 3-D Carbon Nanotube Solid Networks" (Award FA9550-12-1-0035). R.M.Y. acknowledges the financial support from UGC, Govt. of India, for the Raman Fellowship under Indo-US 21st Century knowledge Initiative. J.W. thanks the BRI funding support from AFOSR (FA9550-14-1-0268). J.L. also acknowledges the support from the Welch foundation C-1716.

■ REFERENCES

(1) Arico, A. S.; Bruce, P.; Scrosati, B.; Tarascon, J.-M.; van Schalkwijk, W. Nanostructured Materials for Advanced Energy Conversion and Storage Devices. *Nat. Mater.* **2005**, *4*, 366−377.

(2) Tian, G.-L.; Zhao, M.-Q.; Yu, D.; Kong, X.-Y.; Huang, J.-Q.; Zhang, Q.; Wei, F. Nitrogen-Doped Graphene/Carbon Nanotube Hybrids: In Situ Formation on Bifunctional Catalysts and Their Superior Electrocatalytic Activity for Oxygen Evolution/Reduction Reaction. *Small* **2014**, *10*, 2251−2259.

(3) Jin, C.; Lu, F.; Cao, X.; Yang, Z.; Yang, R. Facile Synthesis and Excellent Electrochemical Properties of $NiCo_2O_4$ Spinel Nanowire Arrays as a Bifunctional Catalyst for the Oxygen Reduction and Evolution Reaction. *J. Mater. Chem. A* **2013**, *1*, 12170−12177.

(4) Steele, B. C. H.; Heinzel, A. Materials for Fuel-Cell Technologies. *Nature* **2001**, *414*, 345−352.

(5) McCrory, C. C. L.; Jung, S.; Peters, J. C.; Jaramillo, T. F. Benchmarking Heterogeneous Electrocatalysts for the Oxygen Evolution Reaction. *J. Am. Chem. Soc.* **2013**, *135*, 16977−16987.

(6) Ma, T. Y.; Dai, S.; Jaroniec, M.; Qiao, S. Z. Metal−Organic Framework Derived Hybrid Co_3O_4−Carbon Porous Nanowire Arrays as Reversible Oxygen Evolution Electrodes. *J. Am. Chem. Soc.* **2014**, *136*, 13925−13931.

(7) Wu, J.; Zhang, D.; Wang, Y.; Hou, B. Electrocatalytic Activity of Nitrogen-Doped Graphene Synthesized Via a One-Pot Hydrothermal Process towards Oxygen Reduction Reaction. *J. Power Sources* **2013**, *227*, 185−190.

(8) Gewirth, A. A.; Thorum, M. S. Electroreduction of Dioxygen for Fuel-Cell Applications: Materials and Challenges. *Inorg. Chem.* **2010**, *49*, 3557−3566.

(9) Gong, K.; Du, F.; Xia, Z.; Durstock, M.; Dai, L. Nitrogen-Doped Carbon Nanotube Arrays with High Electrocatalytic Activity for Oxygen Reduction. *Science* **2009**, *323*, 760−764.

(10) Yang, D.-S.; Bhattacharjya, D.; Inamdar, S.; Park, J.; Yu, J.-S. Phosphorus-Doped Ordered Mesoporous Carbons with Different Lengths as Efficient Metal-Free Electrocatalysts for Oxygen Reduction Reaction in Alkaline Media. *J. Am. Chem. Soc.* **2012**, *134*, 16127−16130.

(11) Peng, H.; Mo, Z.; Liao, S.; Liang, H.; Yang, L.; Luo, F.; Song, H.; Zhong, Y.; Zhang, B. High Performance Fe- and N-Doped Carbon Catalyst with Graphene Structure for Oxygen Reduction. *Sci. Rep.* **2013**, *3*, 1765.

(12) Wohlgemuth, S.-A.; White, R. J.; Willinger, M.-G.; Titirici, M.-M.; Antonietti, M. A One-Pot Hydrothermal Synthesis of Sulfur and Nitrogen Doped Carbon Aerogels with Enhanced Electrocatalytic Activity in the Oxygen Reduction Reaction. *Green Chem.* **2012**, *14*, 1515−1523.

(13) Zhang, Y.; Ge, J.; Wang, L.; Wang, D.; Ding, F.; Tao, X.; Chen, W. Manageable N-Doped Graphene for High Performance Oxygen Reduction Reaction. *Sci. Rep.* **2013**, *3*, 2771.

(14) Tian, G.-L.; Zhang, Q.; Zhang, B.; Jin, Y.-G.; Huang, J.-Q.; Su, D. S.; Wei, F. Toward Full Exposure of "Active Sites": Nanocarbon Electrocatalyst with Surface Enriched Nitrogen for Superior Oxygen Reduction and Evolution Reactivity. *Adv. Funct. Mater.* **2014**, *24*, 5956−5961.

(15) Yang, S.; Zhi, L.; Tang, K.; Feng, X.; Maier, J.; Müllen, K. Efficient Synthesis of Heteroatom (N or S)-Doped Graphene Based on Ultrathin Graphene Oxide-Porous Silica Sheets for Oxygen Reduction Reactions. *Adv. Funct. Mater.* **2012**, *22*, 3634−3640.

(16) Chen, Z.; Higgins, D.; Yu, A.; Zhang, L.; Zhang, J. A Review on Non-Precious Metal Electrocatalysts for PEM Fuel Cells. *Energy Environ. Sci.* **2011**, *4*, 3167−3192.

(17) Zhao, Y.; Yang, L.; Chen, S.; Wang, X.; Ma, Y.; Wu, Q.; Jiang, Y.; Qian, W.; Hu, Z. Can Boron and Nitrogen Co-doping Improve Oxygen Reduction Reaction Activity of Carbon Nanotubes? *J. Am. Chem. Soc.* **2013**, *135*, 1201−1204.

(18) Zhong, H.; Zhang, H.; Xu, Z.; Tang, Y.; Mao, J. A Nitrogen-Doped Polyaniline Carbon with High Electrocatalytic Activity and Stability for the Oxygen Reduction Reaction in Fuel Cells. *ChemSusChem* **2012**, *5*, 1698−1702.

(19) Sun, X.; Song, P.; Zhang, Y.; Liu, C.; Xu, W.; Xing, W. A Class of High Performance Metal-Free Oxygen Reduction Electrocatalysts based on Cheap Carbon Blacks. *Sci. Rep.* **2013**, *3*, 2505.

(20) Li, J.-S.; Li, S.-L.; Tang, Y.-J.; Li, K.; Zhou, L.; Kong, N.; Lan, Y.-Q.; Bao, J.-C.; Dai, Z.-H. Heteroatoms Ternary-Doped Porous Carbons Derived from MOFs as Metal-Free Electrocatalysts for Oxygen Reduction Reaction. *Sci. Rep.* **2014**, *4*, 5130.

(21) Tuci, G.; Zafferoni, C.; D'Ambrosio, P.; Caporali, S.; Ceppatelli, M.; Rossin, A.; Tsoufis, T.; Innocenti, M.; Giambastiani, G. Tailoring Carbon Nanotube N-Dopants while Designing Metal-Free Electrocatalysts for the Oxygen Reduction Reaction in Alkaline Medium. *ACS Catal.* **2013**, *3*, 2108−2111.

(22) Lin, Z.; Waller, G.; Liu, Y.; Liu, M.; Wong, C.-P. Facile Synthesis of Nitrogen-Doped Graphene via Pyrolysis of Graphene Oxide and Urea, and its Electrocatalytic Activity toward the Oxygen-Reduction Reaction. *Adv. Energy Mater.* **2012**, *2*, 884−888.

DOI: 10.1021/acsami.5b02032
ACS Appl. Mater. Interfaces 2015, 7, 11991−12000

(23) Zhao, Y.; Nakamura, R.; Kamiya, K.; Nakanishi, S.; Hashimoto, K. Nitrogen-Doped Carbon Nanomaterials as Non-Metal Electrocatalysts for Water Oxidation. *Nat. Commun.* **2013**, *4*, 2390.
(24) Lin, Z.; Waller, G. H.; Liu, Y.; Liu, M.; Wong, C.-P. Simple Preparation of Nanoporous Few-Layer Nitrogen-Doped Graphene for use as an Efficient Electrocatalyst for Oxygen Reduction and Oxygen Evolution Reactions. *Carbon* **2013**, *53*, 130−136.
(25) Sharifi, T.; Hu, G.; Jia, X.; Wågberg, T. Formation of Active Sites for Oxygen Reduction Reactions by Transformation of Nitrogen Functionalities in Nitrogen-Doped Carbon Nanotubes. *ACS Nano* **2012**, *6*, 8904−8912.
(26) Niwa, H.; Horiba, K.; Harada, Y.; Oshima, M.; Ikeda, T.; Terakura, K.; Ozaki, J.-i.; Miyata, S. X-Ray Absorption Analysis of Nitrogen Contribution to Oxygen Reduction Reaction in Carbon Alloy Cathode Catalysts for Polymer Electrolyte Fuel Cells. *J. Power Sources* **2009**, *187*, 93−97.
(27) Kundu, S.; Nagaiah, T. C.; Xia, W.; Wang, Y.; Dommele, S. V.; Bitter, J. H.; Santa, M.; Grundmeier, G.; Bron, M.; Schuhmann, W.; Muhler, M. Electrocatalytic Activity and Stability of Nitrogen-Containing Carbon Nanotubes in the Oxygen Reduction Reaction. *J. Phys. Chem. C* **2009**, *113*, 14302−14310.
(28) Rao, C. V.; Cabrera, C. R.; Ishikawa, Y. In Search of the Active Site in Nitrogen-Doped Carbon Nanotube Electrodes for the Oxygen Reduction Reaction. *J. Phys. Chem. Lett.* **2010**, *1*, 2622−2627.
(29) Kaukonen, M.; Kujala, R.; Kauppinen, E. On the Origin of Oxygen Reduction Reaction at Nitrogen-Doped Carbon Nanotubes: A Computational Study. *J. Phys. Chem. C* **2011**, *116*, 632−636.
(30) Yadav, R. M.; Shripathi, T.; Srivastava, A.; Srivastava, O. N. Effect of Ferrocene Concentration on the Synthesis of Bamboo-Shaped Carbon Nitrogen Nanotube Bundles. *J. Nanosci. Nanotechnol.* **2005**, *5*, 820−824.
(31) Davis, R. E.; Horvath, G. L.; Tobias, C. W. The Solubility And Diffusion Coefficient of Oxygen in Potassium Hydroxide Solutions. *Electrochim. Acta* **1967**, *12*, 287−297.
(32) Ratso, S.; Kruusenberg, I.; Vikkisk, M.; Joost, U.; Shulga, E.; Kink, I.; Kallio, T.; Tammeveski, K. Highly Active Nitrogen-Doped Few-Layer Graphene/Carbon Nanotube Composite Electrocatalyst for Oxygen Reduction Reaction in Alkaline Media. *Carbon* **2014**, *73*, 361−370.
(33) Yadav, R.; Dobal, P.; Shripathi, T.; Katiyar, R.; Srivastava, O. Effect of Growth Temperature on Bamboo-Shaped Carbon−Nitrogen (C−N) Nanotubes Synthesized Using Ferrocene Acetonitrile Precursor. *Nanoscale Res. Lett.* **2008**, *4*, 197−203.
(34) Li, Y.; Zhang, X. B.; Tao, X. Y.; Xu, J. M.; Huang, W. Z.; Luo, J. H.; Luo, Z. Q.; Li, T.; Liu, F.; Bao, Y.; Geise, H. J. Mass Production of High-Quality Multi-Walled Carbon Nanotube Bundles on a Ni/Mo/Mgo Catalyst. *Carbon* **2005**, *43*, 295−301.
(35) Tan, P.; An, L.; Liu, L.; Guo, Z.; Czerw, R.; Carroll, D. L.; Ajayan, P. M.; Zhang, N.; Guo, H. Probing the Phonon Dispersion Relations of Graphite from the Double-Resonance Process of Stokes and Anti-Stokes Raman Scatterings in Multiwalled Carbon Nanotubes. *Phys. Rev. B* **2002**, *66*, No. 245410.
(36) Liu, L.; Qin, Y.; Guo, Z.-X.; Zhu, D. Reduction of Solubilized Multi-Walled Carbon Nanotubes. *Carbon* **2003**, *41*, 331−335.
(37) Dresselhaus, M. S.; Jorio, A.; Hofmann, M.; Dresselhaus, G.; Saito, R. Perspectives on Carbon Nanotubes and Graphene Raman Spectroscopy. *Nano Lett.* **2010**, *10*, 751−758.
(38) Zhao, Q.; Wagner, H. D. Raman Spectroscopy of Carbon-Nanotube-Based Composites. *Philos. Trans. R. Soc., A* **2004**, *362*, 2407−2424.
(39) Ma, X.; Wang, E. G.; Tilley, R. D.; Jefferson, D. A.; Zhou, W. Size-Controlled Short Nanobells: Growth and Formation Mechanism. *Appl. Phys. Lett.* **2000**, *77*, 4136−4138.
(40) Zhang, L.; Li, H.; Yue, K.-T.; Zhang, S.-L.; Wu, X.; Zi, J.; Shi, Z.; Gu, Z. Effects of Intense Laser Irradiation on Raman Intensity Features of Carbon Nanotubes. *Phys. Rev. B* **2002**, *65*, No. 073401.
(41) Lee, Y. T.; Kim, N. S.; Bae, S. Y.; Park, J.; Yu, S.-C.; Ryu, H.; Lee, H. J. Growth of Vertically Aligned Nitrogen-Doped Carbon Nanotubes: Control of the Nitrogen Content over the Temperature Range 900−1100 °C. *J. Phys. Chem. B* **2003**, *107*, 12958−12963.
(42) Antunes, E. F.; Lobo, A. O.; Corat, E. J.; Trava-Airoldi, V. J. Influence of Diameter in the Raman Spectra of Aligned Multi-Walled Carbon Nanotubes. *Carbon* **2007**, *45*, 913−921.
(43) Tuci, G.; Zafferoni, C.; Rossin, A.; Milella, A.; Luconi, L.; Innocenti, M.; Truong Phuoc, L.; Duong-Viet, C.; Pham-Huu, C.; Giambastiani, G. Chemically Functionalized Carbon Nanotubes with Pyridine Groups as Easily Tunable N-Decorated Nanomaterials for the Oxygen Reduction Reaction in Alkaline Medium. *Chem. Mater.* **2014**, *26*, 3460−3470.
(44) Rao, C. V.; Ishikawa, Y. Activity, Selectivity, and Anion-Exchange Membrane Fuel Cell Performance of Virtually Metal-Free Nitrogen-Doped Carbon Nanotube Electrodes for Oxygen Reduction Reaction. *J. Phys. Chem. C* **2012**, *116*, 4340−4346.
(45) Cheng, Y.; Zhang, H.; Varanasi, C. V.; Liu, J. Highly Efficient Oxygen Reduction Electrocatalysts Based on Winged Carbon Nanotubes. *Sci. Rep.* **2013**, *3*, 3195.
(46) Greeley, J.; Nørskov, J. K. Combinatorial Density Functional Theory-Based Screening of Surface Alloys for the Oxygen Reduction Reaction. *J. Phys. Chem. C* **2009**, *113*, 4932−4939.
(47) Huang, S.-F.; Terakura, K.; Ozaki, T.; Ikeda, T.; Boero, M.; Oshima, M.; Ozaki, J.-i.; Miyata, S. First-Principles Calculation of the Electronic Properties of Graphene Clusters Doped with Nitrogen and Boron: Analysis of Catalytic Activity for the Oxygen Reduction Reaction. *Phys. Rev. B* **2009**, *80*, No. 235410.
(48) Kim, H.; Lee, K.; Woo, S. I.; Jung, Y. On the Mechanism of Enhanced Oxygen Reduction Reaction in Nitrogen-Doped Graphene Nanoribbons. *Phys. Chem. Chem. Phys.* **2011**, *13*, 17505−17510.
(49) Ouyang, W.; Zeng, D.; Yu, X.; Xie, F.; Zhang, W.; Chen, J.; Yan, J.; Xie, F.; Wang, L.; Meng, H.; Yuan, D. Exploring the Active Sites of Nitrogen-Doped Graphene as Catalysts for the Oxygen Reduction Reaction. *Int. J. Hydrogen Energy* **2014**, *39*, 15996−16005.
(50) Nagaiah, T. C.; Kundu, S.; Bron, M.; Muhler, M.; Schuhmann, W. Nitrogen-Doped Carbon Nanotubes as a Cathode Catalyst for the Oxygen Reduction Reaction in Alkaline Medium. *Electrochem. Commun.* **2010**, *12*, 338−341.
(51) Deng, D.; Pan, X.; Yu, L.; Cui, Y.; Jiang, Y.; Qi, J.; Li, W.-X.; Fu, Q.; Ma, X.; Xue, Q.; Sun, G.; Bao, X. Toward N-Doped Graphene via Solvothermal Synthesis. *Chem. Mater.* **2011**, *23*, 1188−1193.
(52) Wang, P.; Wang, Z.; Jia, L.; Xiao, Z. Origin of the Catalytic Activity of Graphite Nitride for the Electrochemical Reduction of Oxygen: Geometric Factors vs. Electronic Factors. *Phys. Chem. Chem. Phys.* **2009**, *11*, 2730−2740.
(53) Lai, L.; Potts, J. R.; Zhan, D.; Wang, L.; Poh, C. K.; Tang, C.; Gong, H.; Shen, Z.; Lin, J.; Ruoff, R. S. Exploration of the Active Center Structure of Nitrogen-Doped Graphene-Based Catalysts for Oxygen Reduction Reaction. *Energy Environ. Sci.* **2012**, *5*, 7936−7942.
(54) Zhang, L.; Xia, Z. Mechanisms of Oxygen Reduction Reaction on Nitrogen-Doped Graphene for Fuel Cells. *J. Phys. Chem. C* **2011**, *115*, 11170−11176.
(55) Chen, Z.; Higgins, D.; Tao, H.; Hsu, R. S.; Chen, Z. Highly Active Nitrogen-Doped Carbon Nanotubes for Oxygen Reduction Reaction in Fuel Cell Applications. *J. Phys. Chem. C* **2009**, *113*, 21008−21013.
(56) Zhang, B.; Wen, Z.; Ci, S.; Mao, S.; Chen, J.; He, Z. Synthesizing Nitrogen-Doped Activated Carbon and Probing its Active Sites for Oxygen Reduction Reaction in Microbial Fuel Cells. *ACS Appl. Mater. Interfaces* **2014**, *6*, 7464−7470.
(57) Wilder, J. W. G.; Venema, L. C.; Rinzler, A. G.; Smalley, R. E.; Dekker, C. Electronic Structure of Atomically Resolved Carbon Nanotubes. *Nature* **1998**, *391*, 59−62.
(58) Hamada, N.; Sawada, S.-i.; Oshiyama, A. New One-Dimensional Conductors: Graphitic Microtubules. *Phys. Rev. Lett.* **1992**, *68*, 1579−1581.
(59) Saito, R.; Fujita, M.; Dresselhaus, G.; Dresselhaus, M. S. Electronic Structure of Chiral Graphene Tubules. *Appl. Phys. Lett.* **1992**, *60*, 2204−2206.

DOI: 10.1021/acsami.5b02032
ACS Appl. Mater. Interfaces 2015, 7, 11991−12000

(60) Mayrhofer, K. J. J.; Strmcnik, D.; Blizanac, B. B.; Stamenkovic, V.; Arenz, M.; Markovic, N. M. Measurement of Oxygen Reduction Activities via the Rotating Disc Electrode Method: From Pt Model Surfaces to Carbon-Supported High Surface Area Catalysts. *Electrochim. Acta* **2008**, *53*, 3181−3188.
(61) Geng, D.; Chen, Y.; Chen, Y.; Li, Y.; Li, R.; Sun, X.; Ye, S.; Knights, S. High Oxygen-Reduction Activity and Durability of Nitrogen-Doped Graphene. *Energy Environ. Sci.* **2011**, *4*, 760−764.
(62) Liang, H.-W.; Zhuang, X.; Brüller, S.; Feng, X.; Müllen, K. Hierarchically Porous Carbons with Optimized Nitrogen Doping as Highly Active Electrocatalysts for Oxygen Reduction. *Nat. Commun.* **2014**, *5*, 5973.
(63) Liang, Y.; Li, Y.; Wang, H.; Zhou, J.; Wang, J.; Regier, T.; Dai, H. Co_3O_4 Nanocrystals on Graphene as a Synergistic Catalyst for Oxygen Reduction Reaction. *Nat. Mater.* **2011**, *10*, 780−786.
(64) Schmidt, T. J.; Stamenkovic, V.; Arenz, M.; Markovic, N. M.; Ross, P. N., Jr. Oxygen Electrocatalysis in Alkaline Electrolyte: Pt(*hkl*), Au(*hkl*) and the Effect of Pd-Modification. *Electrochim. Acta* **2002**, *47*, 3765−3776.
(65) Blizanac, B. B.; Ross, P. N.; Marković, N. M. Oxygen Reduction on Silver Low-Index Single-Crystal Surfaces in Alkaline Solution: Rotating Ring Disk Ag(*hkl*) Studies. *J. Phys. Chem. B* **2006**, *110*, 4735−4741.
(66) Wu, J.; Xia, F.; Pan, M.; Zhou, X.-D. Oxygen Reduction Reaction on Active and Stable Nanoscale $TiSi_2$ Supported Electrocatalysts. *J. Electrochem. Soc.* **2012**, *159*, B654−B660.
(67) Chen, S.; Duan, J.; Jaroniec, M.; Qiao, S. Z. Three-Dimensional N-Doped Graphene Hydrogel/NiCo Double Hydroxide Electrocatalysts for Highly Efficient Oxygen Evolution. *Angew. Chem., Int. Ed.* **2013**, *52*, 13567−13570.
(68) Chen, S.; Duan, J.; Ran, J.; Jaroniec, M.; Qiao, S. Z. N-Doped Graphene Film-Confined Nickel Nanoparticles as a Highly Efficient Three-Dimensional Oxygen Evolution Electrocatalyst. *Energy Environ. Sci.* **2013**, *6*, 3693−3699.
(69) Mao, S.; Wen, Z.; Huang, T.; Hou, Y.; Chen, J. High-Performance Bi-Functional Electrocatalysts of 3D Crumpled Graphene−Cobalt Oxide Nanohybrids for Oxygen Reduction and Evolution Reactions. *Energy Environ. Sci.* **2014**, *7*, 609−616.

DOI: 10.1021/acsami.5b02032
ACS Appl. Mater. Interfaces 2015, 7, 11991−12000